Performance Assessment of Dual Frequency GBAS Protection Level Algorithms using a Dual Constellation and Non-Gaussian Error Distributions

Patrick Rémi, *German Aerospace Center (DLR)*
Boubeker Belabbas, *German Aerospace Center (DLR)*
Thomas Dautermann, *German Aerospace Center (DLR)*
Michael Meurer, *German Aerospace Center (DLR)*

BIOGRAPHY

Patrick Rémi is a research fellow at the DLR (German Aerospace Center) at the Institute of Communications and Navigation at Oberpfaffenhofen near Munich. He received his diploma in electrical engineering from the Technical University of Munich in 2007. His field of work is the integrity of Ground Based Augmentation Systems.

Boubeker Belabbas is a research fellow at the DLR (German Aerospace Center) at the Institute of Communications and Navigation at Oberpfaffenhofen near Munich. He received his MSc degree in Mechanics and Energetic from the Ecole Nationale Supérieure d'Electricité et de Mécanique at Nancy (France) in 1995 and a specialised "mastère" in Aerospace Mechanics at the Ecole Nationale Supérieure de l'Aéronautique et de l'Espace "SUPAERO" at Toulouse (France) in 2001. His field of work is the integrity of GNSS with its augmentations and its applicability for Safety of Life receivers.

Thomas Dautermann received his Vordiplom in Physics from the Technical University of Kaiserslautern in 2003. In 2004 he obtained a Master of Science degree in Physics from Purdue University, West Lafayette, IN, USA , followed by a PhD titled "Ionospheric Total Electron Content Perturbations Induced by Lithosphere-Atmosphere-Ionosphere Interaction", also from Purdue University. Thomas Dautermann also holds a commercial pilot certificate with instrument privileges. He is the DLR manager for the German national project HETEREX, which deals with GBAS L1 CAT-III automatic landings and a expert in error propagation and integrity assessments.

Michael Meurer received the diploma in Electrical Engineering and the Ph.D. degree from the University of Kaiserslautern, Germany. After graduation, he joined the Research Group for Radio Communications at the Technical University of Kaiserslautern, Germany, as a senior key researcher, where he was involved in various international and national projects in the field of communications and navigation both as project coordinator and as technical contributor. From 2003 till 2005, Dr. Meurer was active as a senior lecturer. Since 2005 he has been an Associate Professor (PD) at the same university. Additionally, since 2006 Dr. Meurer is with the German Aerospace Centre (DLR), Institute for Communications and Navigation, where he is the director of the Department of Navigation.

ABSTRACT

The landing of aircraft under low visibility conditions has always been a challenge even with conventional navigation systems like ILS (Instrument Landing System). The requirements for CAT III can not be reached with Ground Based Augmentation Systems (GBAS) for single frequency GPS only without relaxing the alarm limits and continuity requirements of air navigation. Large delay gradients between the GBAS ground station and the user caused by ionospheric anomalies, remain the main threat for GBAS.
Using GBAS with both GPS and Galileo in a combined constellation will increase the robustness of the complete system. Galileo is providing promising features like the possibility offered to the aviation community to acquire 3 frequencies: L1, E5a and E5b in the Aeronautical Radio Navigation Service (ARNS) band. The consideration of phase observations allows the use of efficient smoothing techniques: the ionosphere free and the divergence free dual frequency smoothing algorithms which have been defined in [1], allow to mitigate or even to cancel the ionosphere gradient. Due to the different geometry characteristic of the extended constellation the Geometry Dilution of Precision (GDOP) is reduced. The low

probability of satellite outages combined with the number of additionally available satellites will dramatically improve the availability of the combined GPS and Galileo system.

The objective of this work is to analyze the impact of Galileo through the use of a combined constellation on the performance of GBAS under severe ionospheric gradients. The errors experienced by a user with a spatial separation of 5km and 20NM respectively to the GBAS ground station are evaluated. The simulation scenario considers an ionosphere anomaly with a gradient of 420mm per km between the ground station and the user – a value which has turned out to be a worst-case assumption as explained before in several publications [2]. The dual frequency smoothing techniques mentioned above are applied.
The simulation is performed over a period of several days to account for the effects of the changing satellite geometry.
The models of the GBAS residual errors used in the preceding work [3] were considered to be Gaussian distributed individual errors. To give a more realistic representation of the individual errors used in the simulation, we use distributions of errors which are, in general not Gaussian. The distributions are derived from measurements or theoretical considerations pertaining to the origin of the error. Here, we consider the four major individual sources of pseudorange error in GBAS systems: receiver noise, ionosphere and troposphere, multipath.
For this work, the impact of applying smoothing filter, averaging and position calculation are taken into account.

INTRODUCTION

It is well known that a severe ionosphere gradient is the main threat for GBAS especially for precision landings with respect to CAT III. The use of dual frequency techniques can mitigate this threat and even suppress it. Two smoothing techniques have been studied in [1]. This paper will investigate the impact of the use of a combined constellation using GPS and Galileo on the errors resulting in different ionosphere gradient scenarios and considering the smoothing techniques defined in [1].

GBAS Architecture

Future GBAS systems will use a multi-frequency multi constellation to enable precision landing of category III. Different configurations are considered but the general architecture standardised in [4] although for single frequency GBAS, will be kept for dual frequency GBAS. It is supposed that the ground subsystem is monitoring both GPS and Galileo constellations and provides the corrections of all satellites in view to the user. A short description of the architecture is presented in the following figure:

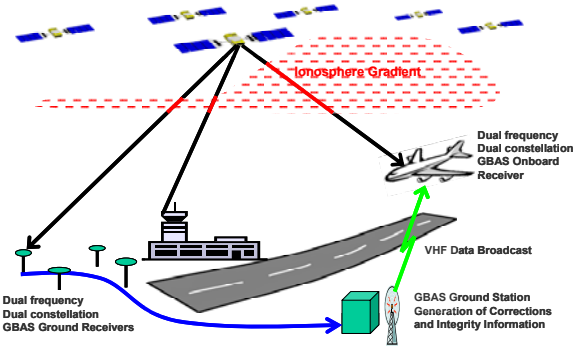

Figure 1: GBAS Architecture

SIMULATION SCENARIO

For the simulations used in this work we considered the position of our GBAS station to be at Oberpfaffenhofen near Munich. We assumed the use of a combined GNSS constellation with 30 satellites in the Galileo and 30 satellites in the GPS constellation, where we used the corresponding signals on L1/E1 and L5/E5a for the dual frequency smoothing algorithms described below. These algorithms were evaluated at a distance of 5km and 20 nautical miles between the user and the GBAS ground station under nominal ionosphere conditions and for severe ionosphere conditions with a ionosphere gradient of 420mm/km.
In order to carry out our considerations under worst case conditions we start with an observation of the number of visible satellites at Oberpfaffenhofen using the combined constellation. Figure 2 shows that the number varies between 15 and 26.

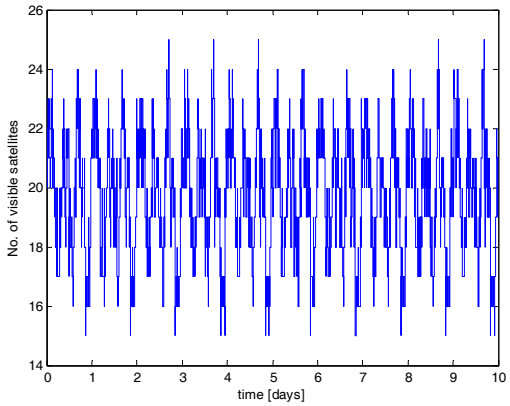

Figure 2: No. of Visible Satellites

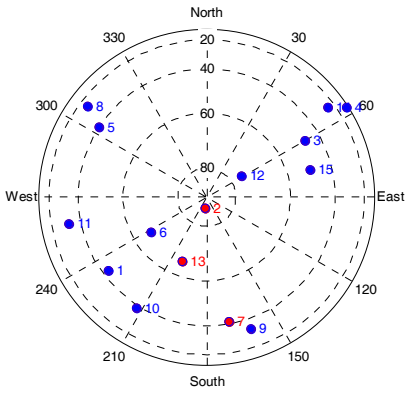

Figure 3: Skyplot for worst VDOP

The worst vertical dilution of precision (VDOP) results for 15 visible satellites. This gives us the geometry shown in figure 3. To evaluate the performance of the smoothing algorithms under severe ionosphere conditions we choose up to 3 satellites which are affected by a ionosphere front. The first satellite selected for this is the one with the strongest influence on the vertical component of the position solution, i.e. the one with biggest entry s_{3j} in the third row of the weighted pseudoinverse matrix S. For the chosen geometry in figure 3 it is satellite no. 2. The second and third satellite are then those satellites which are closest to the first one in terms of azimuth (satellite 7 and 13).

DUAL FREQUENCY SMOOTHING

In this paper, two smoothing techniques defined in [1] are considered: The ionosphere free (I-Free) smoothing and the divergence free (D-Free) smoothing technique. We recall these algorithms below.

Single frequency carrier smoothing

Considering single frequency receivers, it is possible to reduce the noise of the code measurement by filtering with the phase measurement because the phase measurement has a very low level of noise.

The classical low pass filter used can be written as

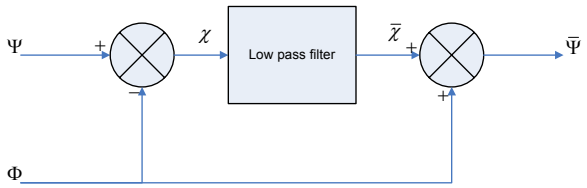

Figure 4: Low pass filter architecture

where
Ψ is the code measurement
Φ is the phase measurement
χ is the input fed in the low pass filter which is for standard single frequency simply the code minus carrier ($\chi = \Psi - \Phi$).

$\bar{\chi}$ is the smoothed χ which can be written in time domain:

$$\bar{\chi}(t+1) = \frac{\tau - 1}{\tau}\bar{\chi}(t) + \frac{1}{\tau}\chi(t+1) \tag{1}$$

Where
τ is the smoothing time constant.

In Laplace domain:

$$\bar{\chi}(s) = F(s)\chi(s) = \frac{1}{\tau s + 1}\chi(s) \tag{2}$$

$\bar{\Psi} = \bar{\chi} + \Phi$ is the smoothed code.

For single frequency carrier smoothing:

$$\begin{aligned} \Psi &= \rho_{L1} = r + I + \eta \\ \Phi &= \phi_{L1} = r - I + N \end{aligned} \tag{3a-b}$$

Where
$\Psi = \rho$ is the code measurement
$\Phi = \phi$ is the phase measurement
r is the geometric range from user to satellite including the troposphere delay and the clock off set.
I is the ionosphere delay
η is the random noise on code measurements and
N is the integer ambiguity of the carrier measurements.

Thus in this case, the input of the low pass filter can be written as follow:

$$\chi = 2I + \eta - N \tag{4}$$

and the smoothed code measurement can be expressed in the Laplace domain as:

$$\bar{\Psi} = r + (2F - 1)I + F\eta \tag{5}$$

Divergence free smoothing

The input to the low pass filter for divergence free smoothing is:

$$\begin{aligned} \Psi_{D-Free} &= \rho_1 \\ \Phi_{D-Free} &= \phi_1 - \frac{2}{\alpha}(\phi_1 - \phi_2) \end{aligned} \tag{6a-b}$$

$$\text{With } \alpha = 1 - \frac{f_1^2}{f_2^2} \tag{7}$$

The smoothed code measurement is:

$$\bar{\Psi}_{D-Free} = r + I_1 + F\eta_1 \tag{8}$$

As it can be seen ionospheric error term is directly passed to the output and is in comparsion to single frequency smoothing not delayed through the smoothing filter.

Ionosphere free smoothing

The input to the low pass filter for ionosphere free smoothing is:

$$\Psi_{I-Free} = \rho_1 - \frac{1}{\alpha}(\rho_1 - \rho_2)$$
$$\Phi_{I-Free} = \phi_1 - \frac{1}{\alpha}(\phi_1 - \phi_2) \quad (9a\text{-}b)$$

The smoothed code measurement is:

$$\bar{\Psi}_{I-Free} = r + F\left(\eta_1 - \frac{1}{\alpha}(\eta_1 - \eta_2)\right) \quad (10)$$

The ionosphere term is removed, at the expense of a higher level of noise in the output.

PSEUDORANGE ERROR MODELS

To analyse the effects of the different smoothing filters, we use the approach taken in [5], i.e. we first choose theoretical probability density functions for the different residual pseudorange error components resulting from multipath, ionosphere gradients, tropospheric delay and receiver noise. We can use a pseudorandom generator based on these pdfs, to generate random samples, which we can pass through the smoothing filters. From this we obtain the post-smoothing pdf using binning. Because we assume the error components to be independent we can combine them to a single pseudorange error pdf by convolution of the individual error component pdfs.

Multipath

The multipath error is distributed according to the following expression given in [6]:

$$p_{mp} = \frac{1}{b^2} \ln \frac{1 + \sqrt{1 - \left(\frac{\varepsilon - a}{b}\right)^2}}{\frac{|\varepsilon - a|}{b}} \quad (11)$$

For this model it is assumed that the phase shift between the reflected signal and the original signal is uniformly distributed. As it can be seen in figure 5, we chose a maximal multipath *b* of 3m and a bias *a* of the distribution of 0.5m.

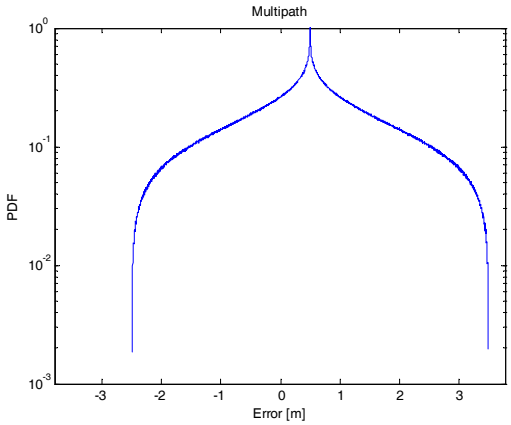

Figure 5: Multipath Error PDF

Ionosphere

For the representation of the residual ionospheric error under nominal ionosphere conditions we follow the work from Mayer [7]. The exponential distribution of the vertical ionosphere gradient y in mm/km is given by the following expression:

$$p_{iono\_vert}(y) = \frac{\ln(10)}{26} 10^{-\frac{|y|}{13}} \quad (12)$$

If we evaluate this expression for a certain distance between user and ground station we get the distribution shown in figure 6 (here for a distance of 5km).

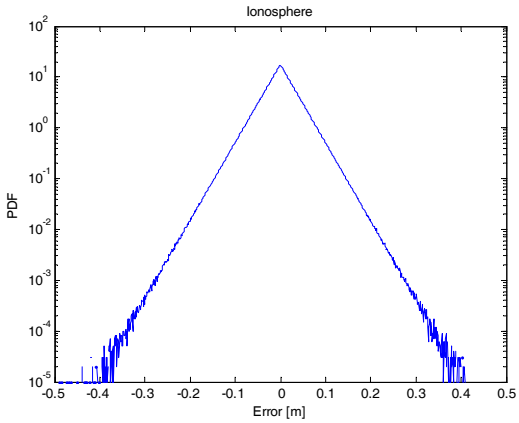

Figure 6: Ionosphere Error PDF

Troposphere

The residual troposphere error is represented by the model given in RTCA DO245a, Section 3.3.2.14, which is a Gaussian distribution, whose standard deviation depends on humidity, satellite elevation angle and altitude difference between user and ground station. Figure 7 shows the corresponding pdf for a satellite elevation of 5°and a distance of 5km between user and ground station with a glide path angle of 3° which corresponds to an altitude of 262m.

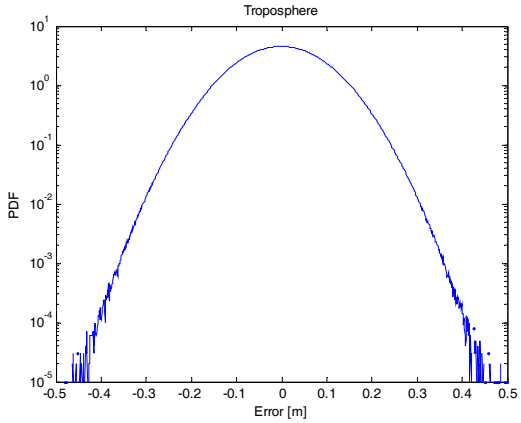

Figure 7: Troposphere Error PDF

Noise

The receiver noise distribution modell is considered to be Gaussian distributed. To distinguish between the different signals on E1, L1, E5a and L5, we calculated the standard deviation according to [8]:

Signal	σ_{noise} [cm]
E1 (MBOC)	11.1
L1 (BPSK(1))	23.8
E5a (BPSK(10))	7.83
L5 (BPSK(10))	7.83

Table 1: Sigmas of the Receiver Noise

Figure 8 shows the noise pdf of the combination of E1 and E5a for the ionosphere free combination before smoothing:

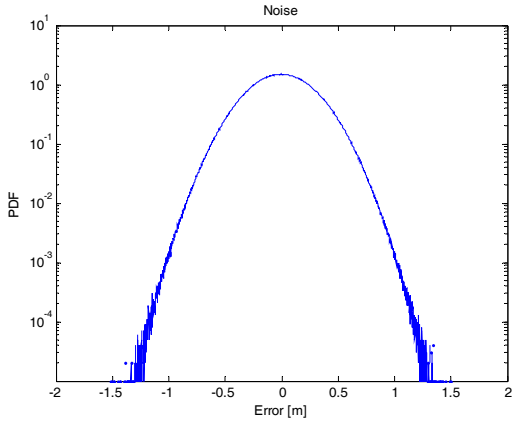

Figure 8: Noise PDF

Pseudorange Error PDF

The resulting residual pseudorange error pdf for a distance of 5km to the ground station is shown in figure 9.

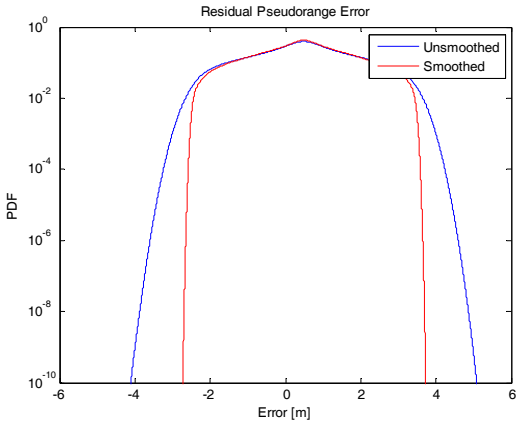

Figure 9: Residual Pseudorange Error PDF Using I-Free Smoothing

The figure shows the pdf for a Galileo satellite at an elevation angle of 5° before and after using ionosphere free smoothing. As it can be seen the variance of the pdf is reduced through the smoothing filter, but the bias induced by the contribution of the multipath error is still present.

POSITION ERROR LEVEL

In the next step we map the obtained pseudorange error distributions to the position domain as described in [5] according to the geometry described in our simulation scenario above. The errors in the pseudorange domain $\varepsilon_{\hat{\rho}}$ are mapped to the position domain using the weighted pseudo-inverse matrix S:

$$\varepsilon_x = S\varepsilon_{\hat{\rho}} \tag{13}$$

Where

$$S = \left(G^T W G\right)^{-1} G^T W \tag{14}$$

With the geometry matrix G and the weighting matrix W.
This mapping can directly be done with the pseudorange error pdfs using the following formula:

$$p(\varepsilon_{i,j}) = \frac{1}{|S_{ij}|} p\left(\frac{\varepsilon_{\rho,j}}{S_{ij}}\right) \tag{15}$$

Where the index i represents the corresponding position coordinate and the index j the number of the corresponding satellite. If we assume the pseudorange errors to be independent, we can convolve the

distributions of all satellites to obtain the error distribution in the position domain.

I-Free vs. D-Free

First we take a look at the results for both smoothing algorithms under nominal ionosphere conditions at a distance of 5km and 20NM. Figure 10 shows these results for the up component of the position error. At first glance we see the effect of the higher noise contribution on the position error when using ionosphere free smoothing. The distribution of errors for divergence free smoothing at both evaluated distances is considerably narrower than the corresponding ones for ionosphere free smoothing. Although residual ionospheric and residual tropospheric errors are still present in the output of the D-Free filter, the effect on the position error at larger distance is small, as it can been seen from the small separation between the D-Free distributions at 5km and 20NM respectively. With the ionospheric error removed in I-Free smoothing the only error component dependent on the spatial separation between user and ground station remaining is the residual tropospheric delay. As it can be seen the dependency on the distance to ground station is even smaller so that the difference is not visible in this plot.

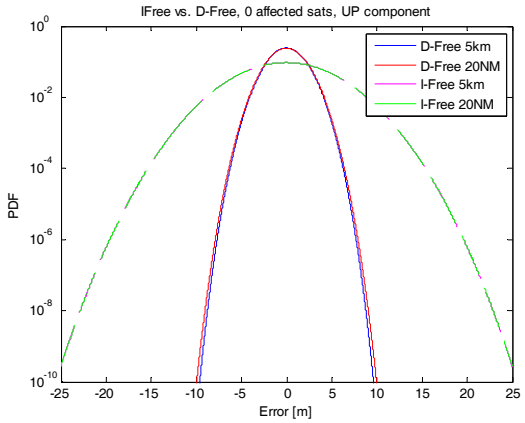

Figure 10: Position error under nominal ionosphere conditions at a distance of 5km and 20NM

D-Free under severe ionosphere conditions

Next we take a look at the results of our simulations for severe ionosphere conditions. As I-Free smoothing is of course not affected by ionosphere fronts it not considered further in this part.
First we take a look at the north component of the position error using D-Free smoothing with 1 to 3 satellites affected by ionospheric front compared to 0 satellites affected by the front (which corresponds to the nominal case). While the effect of the strong ionosphere gradient is only slightly visible in the distiributions at 5km distance, we can see that it results in strong bias of the distribution at 20NM distance for the case of 3 affected satellites.

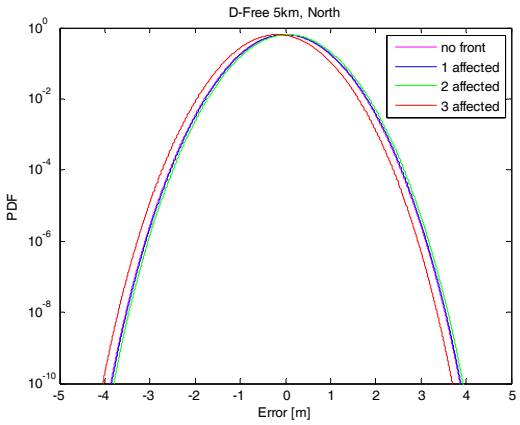

Figure 11: North Component Position Error using D-Free Smoothing under severe ionosphere conditions at a distance of 5km

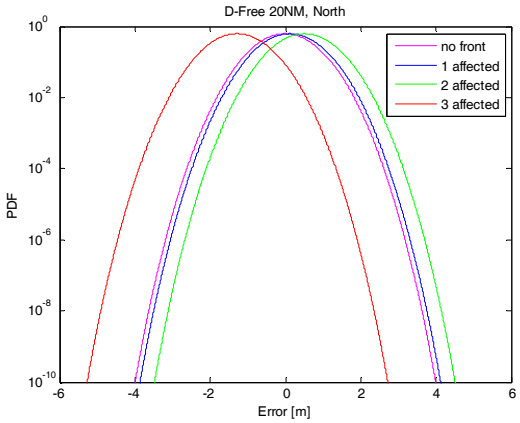

Figure 12: North Component of Position Error using D-Free Smoothing under severe ionosphere conditions at a distance of 20NM

As it could be expected from our choice of the worst VDOP geometry the up component is most affected by the ionosphere front. A bias in the distributions is already visible for a distance of 5km (figure 13), and amounts to more than 17m at a distance of 20NM (figure 14).

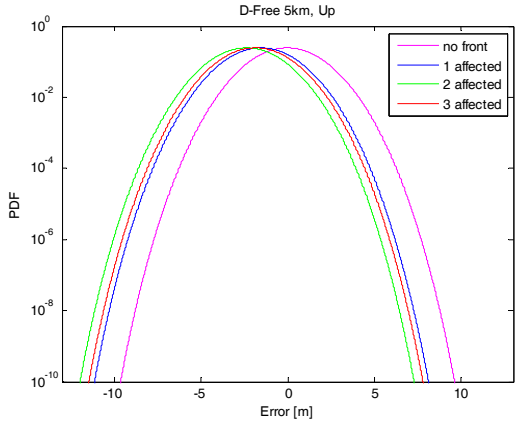

Figure 13: Up Component of Position Error using D-Free Smoothing under severe ionosphere conditions at a distance of 5km

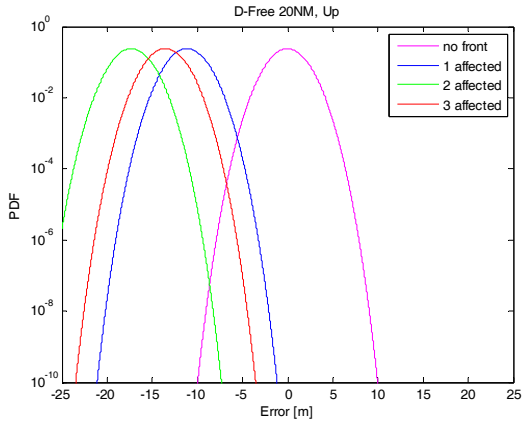

Figure 14: Up Component of Position Error using D-Free Smoothing under severe ionosphere conditions at a distance of 20NM

It is interesting to see that the case with 3 affected satellites doesn't represent the worst case here because we obtain a stronger bias already if only 2 satellites are affected. This is due to our selection of satellites affected by the ionospheric front.

Table 2 shows the S-matrix entries of the affected satellites for the east, north and up direction. The order of the columns corresponds to the order we use when an increasing number of satellites is affected and the numbering corresponds to the numbering given in figure 3.

	Sat. 2	Sat. 13	Sat. 7
East	-0.566	0.1233	0.2845
North	0.0085	0.0247	-0.1150
Up	-0.7157	-0.3962	0.2431

Table 2: S-Matrix Entries of Affected Satellites

As it can be seen the entries of satellite 2 and 13 for the vertical components both have a negative sign. Thus the effect of a bias introduced by these two satellites is partially cancelled when we consider satellite 7 as a third affected satellite, because its entry is positive.

CONCLUSION

The divergence free smoothing technique achieves comparable accuracy as the single frequency smoothing with a higher robustness against temporal ionospheric gradients. Although the ionospheric error is completely removed in ionosphere free smoothing, divergence free smoothing remains a better choice even up to higher levels of ionosphere storms. This is due to fact that the ionosphere free solution suffers from higher noise and multipath contribution because of the combination of code observables for both frequencies. Future work has to show up to which gradients the use of the D-Free solutions is possible and how these gradients can be monitored.

Although we used generalized non-Gaussian distributions to model the individual residual errors the resulting position errors appear to be Gaussian distributed. The level of the error obtained using ionosphere free smoothing is highly dependent on the level of multipath error. In this work we have used a generic multipath model. In future work it needs to be validated with respect to a real multipath environment.

REFERENCES

[1] H. Konno, S. Pullen, J. Rife, P, Enge, "Evaluation of Two Types of Dual-Frequency Differential GPS Techniques under Anomalous Ionosphere Conditions", Proceedings of ION NTM 2006, Monterey, California, Jan. 2006.

[2] S. Ramakrishnan, J. Lee, S. Pullen, P. Enge, "Targeted Ephemeris Decorrelation Parameter Inflation for Improved LAAS Availability during Severe Ionosphere Anomalies", Proceedings of ION NTM 2008, San Diego, California, Jan. 2008

[3] B. Belabbas, P. Rémi, M. Meurer, "Performance Assessment of GBAS CAT III using GPS and Galileo", Proceedings of ION GNSS 2008, Savannah, Georgia, Sept. 2008

[4] Minimum Aviation System Performance Standards for Local Area Augmentation System (LAAS). Washington D.C., RTCA SC-159, WG-4A, DO-245A, December 9, 2004.

[5] T. Dautermann, B. Belabbas, P. Rémi. A Novel Integrity Concept for GBAS Precision Approaches Induced by Error Propagtion with Non-Gaussian Distributions. ENC GNSS 2009, Naples, Italy, May 2009.

[6] B. Pervan, S. Pullen, and I. Sayim. Sigma Estimation, Inflation, and Monitoring in the LAAS Ground System. In ION GPS, 2000.

[7] C. Mayer, N. Jakowski, C. Borries, T. Pannowitsch, and B. Belabbas. Extreme ionospheric conditions over Europe observed during the last solar cycle. In *Navitec*, number S08-01. European Space Agency, 2008.

[8] P. Henkel, V. Gomez, C. Günther. Modified LAMBDA for Absolute Carrier Phase Positioning in the presence of biases. Proceedings of ION NTM 2009, Anaheim, California, Jan 2009.